

# Equivalent Circuit Model for Si Avalanche Photodetectors Fabricated in Standard CMOS Process

Myung-Jae Lee, *Student Member, IEEE*, Hyo-Soon Kang, *Student Member, IEEE*, and Woo-Young Choi, *Member, IEEE*

**Abstract**—We present an equivalent circuit model for CMOS-compatible avalanche photodetectors. The equivalent circuit model includes an inductive component for avalanche delay, a current source for photogenerated carriers, and several components that model the device structure and parasitic effects. The model provides accurate impedance characteristics and photodetection frequency responses.

**Index Terms**—Avalanche photodetector, CMOS, equivalent circuit model, RF peaking.

## I. INTRODUCTION

PHOTODETECTORS based on CMOS technology can provide a cost-effective solution for short-distance optical communications [1] and fiber-supported microwave/millimeter-wave systems [2]. However, they have the inherent drawback of low bandwidth-efficiency product, owing to the narrow depletion region caused by high doping profile [1]. CMOS-compatible avalanche photodetectors (CMOS-APDs) with their internal gain can overcome this drawback. In addition, their speed performance can be enhanced by utilizing the RF-peaking effect [3], which has been observed in several types of APDs [4]–[6]. Although InAlAs/InGaAs- [5] and Si/SiGe-based [6] APDs have the advantage of higher bandwidth-efficiency product, CMOS-APDs can provide a monolithic optical receiver solution based on powerful CMOS technology.

In this letter, we introduce an equivalent circuit model for CMOS-APDs. The model includes an inductive component to account for avalanche delay, a current source for photogenerated carriers, and various elements that model the device structure and parasitic effects. The equivalent circuit parameters are extracted from the impedance characteristics and photodetection frequency response measurements. Good agreement between measurement and simulation results based on the model is achieved. Using the model, we identify the dominant bandwidth limiting factor and clarify the RF-peaking effect in CMOS-APD.

Manuscript received April 12, 2008. Current version published September 24, 2008. This work was supported by the Ministry of Information and Communication (MIC), Korea, under the Information Technology Research Center (ITRC) support program supervised by the Institute of Information Technology Advancement (IITA). The review of this letter was arranged by Prof. P. K.-L. Yu.

The authors are with the Department of Electrical and Electronic Engineering, Yonsei University, Seoul 120-749, Korea (e-mail: fodlmj@yonsei.ac.kr; hkang@yonsei.ac.kr; wchoi@yonsei.ac.kr).

Color versions of one or more of the figures in this letter are available online at <http://ieeexplore.ieee.org>.

Digital Object Identifier 10.1109/LED.2008.2000717

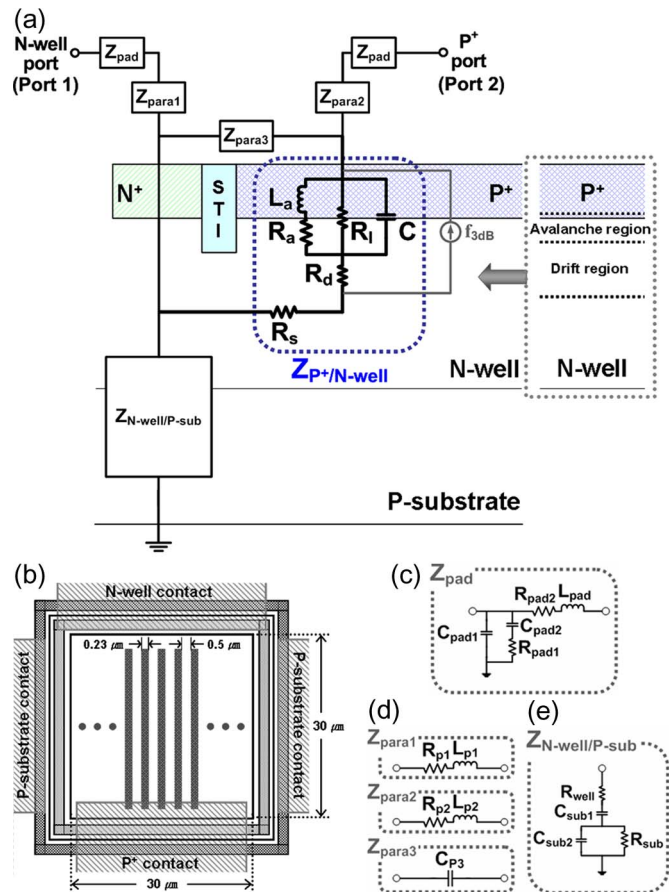


Fig. 1. (a) CMOS-APD structure and equivalent circuit model. (b) Top view of the fabricated CMOS-APD. (c) Equivalent circuit for pads and interconnection lines. (d) Equivalent circuits for the parasitic elements. (e) Equivalent circuit for N-well/P-substrate junction.

## II. STRUCTURE AND MODEL OF CMOS-APD

The CMOS-APD used in our investigation is fabricated in 0.18- $\mu\text{m}$  standard CMOS process without any process modification or special substrates. Fig. 1(a) shows the CMOS-APD structure, as well as the equivalent circuit model blocks. CMOS-APD is implemented by using the vertical P–N junction formed by P+ source/drain to N-well region, and photogenerated signals are extracted from multifinger electrodes in the P+ region to eliminate the slow current generated in N-well/P-substrate junction. Fig. 1(b) schematically shows the device top view. The detailed device structure can be found in [3].

The  $Z_{P^+/N\text{-well}}$  block in Fig. 1(a) represents the circuit model for  $P^+/N\text{-well}$  junction. The depletion region of  $P^+/N\text{-well}$  junction consists of the narrow avalanche region near the metallurgical junction and the drift region in the  $N\text{-well}$  side. This  $P^+/N\text{-well}$  junction is a one-sided abrupt  $P^+/N$  junction, as in the IMPACT ionization Avalanche Transit Time (IMPATT) diode structure [7]. Consequently, the ac conduction current in the avalanche region experiences 90° phase delay to the ac voltage, as in IMPATT diodes. Thus,  $Z_{P^+/N\text{-well}}$  includes an inductive component with inductance  $L_a$  given as

$$L_a = \tau_a / (2\alpha' I_0) \quad (1)$$

where  $\tau_a$  is the transit time across the avalanche region,  $\alpha'$  is the derivative of the ionization coefficient with respect to the electric field, and  $I_0$  is the bias current [7]. For the dissipative effect due to the finite reverse saturation current and the field-dependent velocity, series, and parallel resistors,  $R_a$  and  $R_l$  are also included in  $Z_{P^+/N\text{-well}}$  [8], respectively. The total depletion capacitance between  $P^+$  and  $N\text{-well}$  can be given as  $C = \epsilon_s A / W_D$ , and the drift region resistance can be approximated with  $R_d \approx W_d / 2A\epsilon_s\nu_s$ , where  $\epsilon_s$  is the semiconductor permittivity,  $A$  is the cross-sectional area,  $W_D$  is the depletion region width,  $W_d$  is the drift region width, and  $\nu_s$  is the saturation velocity [7].  $R_s$  models the inactive region resistance in the low doped  $N\text{-well}$  [7].

$Z_{\text{pad}}$  represents the circuit model for pad and interconnection lines, and the details are shown in Fig. 1(c). The pad is implemented by using a ground shield with the bottom metal layer under the signal pad. In  $Z_{\text{pad}}$ ,  $C_{\text{pad1}}$  represents the capacitance between signal pad and bottom metal layer [9], and  $C_{\text{pad2}}$  and  $R_{\text{pad1}}$  are caused by signal leakages from signal pad to substrate.  $R_{\text{pad2}}$  and  $L_{\text{pad}}$  are the parasitic resistance and inductance due to interconnection lines.  $Z_{\text{para1}}$ ,  $Z_{\text{para2}}$ , and  $Z_{\text{para3}}$  are modeled, as shown in Fig. 1(d). The resistance and inductance in  $Z_{\text{para1}}$  and  $Z_{\text{para2}}$  are caused by metal connection for  $N\text{-well}$  and multifinger electrode for  $P^+$  contacts, respectively, and  $Z_{\text{para3}}$  represents the capacitance between  $N^+$  and  $P^+$  electrodes.  $Z_{N\text{-well}/P\text{-sub}}$  represents the circuit model for  $N\text{-well}/P\text{-substrate}$  junction, as shown in Fig. 1(e), where  $R_{\text{well}}$  is the  $N\text{-well}$  region resistance,  $C_{\text{sub1}}$  is the capacitance between  $N\text{-well}$  and  $P\text{-substrate}$ , and  $C_{\text{sub2}}$  and  $R_{\text{sub}}$  are caused by the parasitic effects of Si substrate [10].

When optical signals are illuminated to CMOS-APD, a considerable amount of photons passes through the  $P^+/N\text{-well}$  depletion region, and then, they are absorbed in the charge neutral region or the  $N\text{-well}/P\text{-substrate}$  depletion region due to the large penetration depth of about 14  $\mu\text{m}$  at 850 nm in Si [1]. The slow diffusion currents generated in the charge neutral  $N\text{-well}$  region limit CMOS-APD speed performance. This effect can be modeled with transit-time constant  $\tau_{\text{tr}}$ , which is incorporated into the model by using a current source having single-pole frequency response with  $f_{3dB} \approx (1/(2\pi\tau_{\text{tr}}))$ , as shown in Fig. 1(a) [11].

### III. MEASUREMENT AND PARAMETER EXTRACTION

Using the equivalent circuit model, we performed parameter extraction from the measurement of two-port  $S$ -parameters

TABLE I  
EXTRACTED PARAMETERS FOR  $Z_{\text{pad}}$ ,  $Z_{\text{para1,2,3}}$ , AND  $Z_{N\text{-well}/P\text{-sub}}$

$Z_{\text{pad}}$		$Z_{\text{para1, 2, 3}}$		$Z_{N\text{-well}/P\text{-sub}}$	
$C_{\text{pad1}}$ [fF]	55	$R_{\text{p1}}$ [ $\Omega$ ]	10	$R_{\text{well}}$ [ $\Omega$ ]	30
$C_{\text{pad2}}$ [fF]	5	$L_{\text{p1}}$ [nH]	0.1	$C_{\text{sub1}}$ [fF]	300
$R_{\text{pad1}}$ [k $\Omega$ ]	2.5	$R_{\text{p2}}$ [ $\Omega$ ]	22	$C_{\text{sub2}}$ [fF]	200
$R_{\text{pad2}}$ [ $\Omega$ ]	1	$L_{\text{p2}}$ [nH]	0.1	$R_{\text{sub}}$ [ $\Omega$ ]	280
$L_{\text{pad}}$ [pH]	35	$C_{\text{p3}}$ [fF]	210		

TABLE II  
EXTRACTED PARAMETERS FOR  $Z_{P^+/N\text{-well}}$  AND THE CURRENT SOURCE

	0.3 mA	0.4 mA	0.5 mA
$L_a$ [nH]	14	10.5	8.4
$R_a$ [ $\Omega$ ]	105	50	25
$R_l$ [ $\Omega$ ]	780	540	410
$C$ [fF]	190	190	190
$R_d$ [ $\Omega$ ]	4.2	4.2	4.2
$R_s$ [ $\Omega$ ]	40	40	40
$\tau_{\text{tr}}$ [ps]	135	173	196.5
$f_{3dB}$ [GHz]	1.18	0.92	0.81

and the photodetection frequency responses of CMOS-APD at three different bias currents  $I_0 = 0.3, 0.4,$  and  $0.5$  mA. These bias conditions are around the maximum avalanche gain condition. The current bias was used instead of the voltage bias because it gives finer resolution around the maximum avalanche gain condition, where currents change rapidly. Two-port  $S$ -parameter measurements were performed by using a vector network analyzer under 1-mW optical illumination. An 850-nm laser diode and a 20-GHz electrooptic modulator were used for optical signal generation. For  $S$ -parameter simulation and parameter optimization of the equivalent circuit, Advanced Design System by Agilent Technology was used.

From the measured two-port  $S$ -parameters,  $Y$ - and  $Z$ -parameters were calculated. For extracting  $Z_{\text{pad}}$  parameters, open and short test patterns fabricated with CMOS-APD on the same substrate were used.  $Z_{\text{pad}}$  was extracted from the real and imaginary parts of  $Y$ -parameters of open and short test patterns, and the results are shown in Table I. After deembedding  $Z_{\text{pad}}$ , parameters for  $Z_{\text{para1}}$  and  $Z_{N\text{-well}/P\text{-sub}}$  were obtained by deembedded  $Z_{11} - Z_{12}$  and  $Z_{12}$ , respectively. Parameters for  $Z_{\text{para2}}$  were initially set to the same as those for  $Z_{\text{para1}}$ , and  $Z_{\text{para3}}$  parameters were calculated from the layout dimensions of metal layers. These were later refined by parameter tuning and optimization based on the comparison of measured and simulated reflection coefficients. The resulting parameter values are shown in Table I. All these parameters were assumed independent of bias currents.

For  $Z_{P^+/N\text{-well}}$ ,  $L_a$ ,  $C$ , and  $R_d$  were first calculated from the earlier explained equations. In these calculations, values for doping concentration, depletion region width, avalanche region width, and carrier saturation velocity were estimated from the measured avalanche breakdown voltage of 10.25 V [7].  $R_a$ ,  $R_l$ , and  $R_s$  were determined by the deembedded  $Z_{22} - Z_{12}$  through the fitting process. These values were also refined by parameter tuning and optimization based on the comparison of measured and simulated reflection coefficients. Table II shows the values for  $Z_{P^+/N\text{-well}}$  at three different bias currents  $I_0 = 0.3, 0.4,$  and  $0.5$  mA.  $L_a$  is inversely proportional to the bias current, as determined by (1).  $R_a$  and  $R_l$  decrease as the

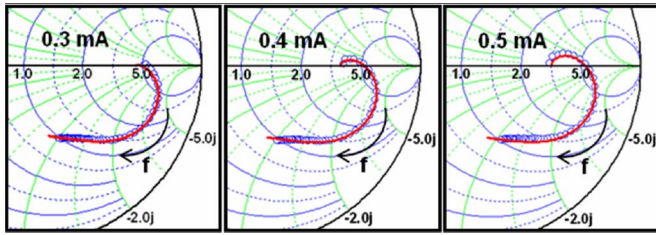


Fig. 2. Measured and fitted reflection coefficients of CMOS-APD at  $P^+$  port under 1-mW optical illumination (from 50 MHz to 13.5 GHz). Hollow circles represent the measured data and solid lines as the fitted results.

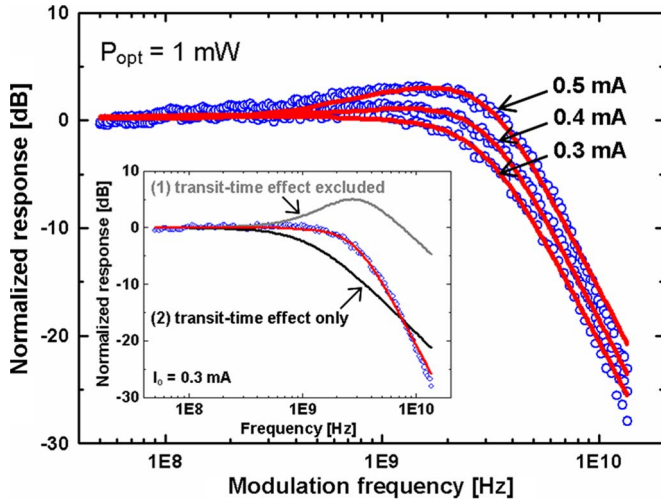


Fig. 3. Measured and fitted photodetection frequency responses of CMOS-APD. The symbols represent the measured data and solid lines as the fitted results. The inset shows the normalized responses at a bias current of 0.3 mA (1) without the transit-time effect and (2) with only the transit-time effect.

bias current increases, which is similar to the results in [8].  $C$ ,  $R_d$ , and  $R_s$  are dependent on the depletion, drift, and inactive region width, respectively, but they change very little at the three bias conditions. Consequently, they were assumed independent of the bias condition. Fig. 2 shows the magnified images of the measured and fitted reflection coefficients of CMOS-APD at  $P^+$  port on the Smith chart at three different bias currents.

Using photodetection frequency responses from the measurement and simulation based on the earlier determined equivalent circuit model including the current source,  $\tau_{tr}$  and  $f_{3dB}$  at three different bias conditions were determined, and the results are shown in Table II. The hole diffusion time in N-well can be estimated as  $\tau_d = 4L^2/(\pi^2D) \approx 160$  ps, using  $L \approx 0.55$   $\mu\text{m}$  and  $D \approx 7.8$   $\text{cm}^2/\text{s}$  [7], confirming that the  $\tau_{tr}$  values given in Table II are reasonable. Fig. 3 shows the normalized measured and fitted photodetection frequency responses of CMOS-APD. The bandwidth enhancement with the bias current increase is due to the increase in the RF-peaking frequency. The inductance decreases with the bias current, as shown in Table II, and the RF-peaking frequency is inversely proportional to the square root of inductance from the  $LC$  resonance condition. Consequently, the RF-peaking frequency increases with the bias current, causing the bandwidth enhancement.

The speed performance of our device is expected to suffer from slow hole diffusion through the N-well, and the degree of

speed limitation by this transit-time effect can be easily investigated by the equivalent circuit model. The inset in Fig. 3 shows the simulation results for the case of 0.3-mA bias current (1) without the transit-time effect obtained by using a frequency-independent current source in the model and (2) with only the transit-time effect obtained by using only the frequency-dependent current source without any other equivalent circuit blocks. When these results are compared with the measurement result, it can be easily observed that the transit-time effect is the dominant cause of speed limitation in our device. The fact that the device bandwidth is actually better than that limited by the transit-time effect is due to the RF-peaking effect in CMOS-APD.

#### IV. CONCLUSION

We present an equivalent circuit model for CMOS-APDs. The equivalent circuit model includes an inductive component and a current source for avalanche delay and photogenerated carriers, respectively. The model also includes several components that represent the CMOS-APD structure and parasitic effects. The model parameter values are extracted from the two-port  $S$ -parameters and the photodetection frequency responses of CMOS-APD. With the model, hole transit time through N-well is identified as the dominant speed limiting factor in CMOS-APD. The RF-peaking effect can compensate this limitation to a certain degree. This equivalent circuit model can be very useful for designing monolithic optical receivers having photodetectors, as well as all the necessary electronic circuits in standard CMOS process.

#### REFERENCES

- [1] T. K. Woodward and A. V. Krishnamoorthy, "1-Gb/s integrated optical detectors and receivers in commercial CMOS technologies," *IEEE J. Sel. Topics Quantum Electron.*, vol. 5, no. 2, pp. 146–156, Mar./Apr. 1999.
- [2] H.-S. Kang and W.-Y. Choi, "Millimeter-wave optoelectronic mixers based on CMOS-compatible Si photodetectors," in *Proc. Int. Top. Meeting Microw. Photon.*, Oct. 2006, pp. 1–4.
- [3] H.-S. Kang, M.-J. Lee, and W.-Y. Choi, "Si avalanche photodetectors fabricated in standard complementary metal–oxide–semiconductor process," *Appl. Phys. Lett.*, vol. 90, no. 15, pp. 151 118–1–151 118–3, Apr. 2007.
- [4] K. M. Johnson, "High-speed photodiode signal enhancement at avalanche breakdown voltage," *IEEE Trans. Electron Devices*, vol. ED-12, no. 2, pp. 55–63, Feb. 1965.
- [5] G. Kim, I. G. Kim, J. H. Baek, and O. K. Kwon, "Enhanced frequency response associated with negative photoconductance in an InGaAs/InAlAs avalanche photodetector," *Appl. Phys. Lett.*, vol. 83, no. 6, pp. 1249–1251, Aug. 2003.
- [6] J.-W. Shi, Y.-S. Wu, Z.-R. Li, and P.-S. Chen, "Impact-ionization-induced bandwidth-enhancement of a Si-SiGe-based avalanche photodiode operating at a wavelength of 830 nm with a gain-bandwidth product of 428 GHz," *IEEE Photon. Technol. Lett.*, vol. 19, no. 7, pp. 474–476, Apr. 2007.
- [7] S. M. Sze and K. K. Ng, *Physics of Semiconductor Devices*, 3rd ed. Hoboken, NJ: Wiley, 2007.
- [8] Y.-C. Wang, "Small-signal characteristics of a Read diode under conditions of field-dependent velocity and finite reverse saturation current," *Solid State Electron.*, vol. 21, no. 4, pp. 609–615, Apr. 1978.
- [9] A. Aktas and M. Ismail, "Pad de-embedding in RF CMOS," *IEEE Circuits Devices Mag.*, vol. 17, no. 3, pp. 8–11, May 2001.
- [10] Y. Ahn, K. Han, and H. Shin, "A new physical RF model of junction varactors," *Jpn. J. Appl. Phys.*, vol. 42, no. 4B, pp. 2110–2113, Apr. 2003.
- [11] G. Wang, T. Tokumitsu, I. Hanawa, K. Sato, and M. Kobayashi, "Analysis of high speed p-i-n photodiodes  $S$ -parameters by a novel small-signal equivalent circuit model," *IEEE Microw. Wireless Compon. Lett.*, vol. 12, no. 10, pp. 378–380, Oct. 2002.